Rapid Communications

Three-dimensional electron-hole superfluidity in a superlattice close to room temperature

M. Van der Donck,[1,*] S. Conti,[1,2] A. Perali,[3,4] A. R. Hamilton,[4] B. Partoens,[1] F. M. Peeters,[1] and D. Neilson[1,4]

[1]*Department of Physics, University of Antwerp, Groenenborgerlaan 171, 2020 Antwerp, Belgium*

[2]*Physics Division, School of Science and Technology, Università di Camerino, 62032 Camerino (MC), Italy*

[3]*Supernano Laboratory, School of Pharmacy, Università di Camerino, 62032 Camerino (MC), Italy*

[4]*ARC Centre of Excellence for Future Low Energy Electronics Technologies, School of Physics, The University of New South Wales, Sydney, N.S.W. 2052, Australia*

(Received 31 October 2019; revised 12 August 2020; accepted 16 August 2020; published 25 August 2020)

Although there is strong theoretical and experimental evidence for electron-hole superfluidity in separated sheets of electrons and holes at low T, extending superfluidity to high T is limited by strong two-dimensional fluctuations and Kosterlitz-Thouless effects. We show this limitation can be overcome using a superlattice of alternating electron- and hole-doped semiconductor monolayers. The superfluid transition in a three-dimensional superlattice is not topological, and for strong electron-hole pair coupling, the transition temperature T_c can be at room temperature. As a quantitative illustration, we show T_c can reach 270 K for a superfluid in a realistic superlattice of transition metal dichalcogenide monolayers.

DOI: 10.1103/PhysRevB.102.060503

It was predicted half a century ago that bound pairs of electrons and holes (excitons) in a semiconductor should quantum condense at low temperatures [1]. To prevent fast electron-hole (e-h) recombination, the electrons and holes can be confined in two spatially separated two-dimensional (2D) layers [2]. At atomically small layer separations, the attractive Coulomb interaction is strong and e-h binding energies in excess of 1000 K have been demonstrated [3]. Under appropriate conditions, these indirect excitons are predicted to form a superfluid condensate with a large energy gap [4,5]. Enhanced tunneling has been observed in e-h double bilayers [6] at transition temperatures $T_c \sim 1$ K. Such enhancement of tunneling is a strong indication of superfluidity or Bose-Einstein condensation (BEC) [7]. A dramatic increase in T_c was recently reported with the observation of enhanced tunneling up to $T_c \sim 100$ K in a double-monolayer transition metal dichalcogenide (TMD) heterostructure [8,9], in good agreement with recent predictions [10].

One might reasonably expect that the transition temperature could be further increased up to the limit set by the large pair binding energies ∼1000 K and the large superfluid gaps ≫300 K. However, any further increase of the transition temperature in these quasi-2D systems is blocked by the Mermin-Wagner theorem [11,12]. Thus the maximum transition temperature is not limited by the e-h binding energy or superfluid gap, but by a Berezinskii-Kosterlitz-Thouless (BKT) topological transition [13]. The transition temperature T^{BKT} is proportional to the carrier density, so it does not increase with coupling strength. Increasing T^{BKT} by increasing the density is not possible, because strong screening of the e-h Coulomb interactions at high densities kills the superfluidity [5,14].

Here, we overcome the restrictions associated with Mermin-Wagner and exploit the strong e-h coupling, by considering superfluidity in a three-dimensional (3D) superlattice, consisting of a stack of alternating electron and hole monolayers. In a 3D system, strong e-h coupling and the associated large superfluid gaps can lead to superfluid transitions at room temperature. We focus specifically on a superlattice of alternating electron-doped and hole-doped monolayers of the transition metal dichalcogenides n-WS_2 and p-WSe_2, but the approach would work for other systems of stacked e-h 2D layers. We note there are already many examples of superlattice-based superconductors [15], including the high-T_c cuprates [16,17].

Figure 1(a) schematically shows the infinite superlattice of alternating n- and p-doped monolayers of two different TMDs, indicated by green and black lines. Within each monolayer, a layer of W transition metal atoms is sandwiched between two layers of S or Se chalcogen atoms. We consider an AA stacked superlattice of WS_2 and WSe_2 monolayers, with the tungsten atoms horizontally aligned, and the chalcogen atoms horizontally aligned [3]. For this stacking, the superlattice has a direct band gap [18]. Electrons and holes generated by the alternate n and p doping of the monolayers form bound pairs. The WS_2/WSe_2 band alignment is type II, which keeps the electrons and the holes spatially separated in their monolayers. This ensures long lifetimes for the interlayer excitons: in a related double-monolayer $MoSe_2/WSe_2$ system, optically generated interlayer excitons with lifetimes ∼1.8 ns have been observed [19]. Since we consider external doping and since the spins of the lowest-energy electrons and holes are opposite (see below), the lifetimes in our system should be an order of magnitude longer than this. Radiative recombination can become relevant at high temperatures and densities, but we find, by considering the interlayer coupling to first order perturbation theory, that the optical transition matrix element for our 3D system is only 1.3 times larger

*matthias.vanderdonck@uantwerpen.be

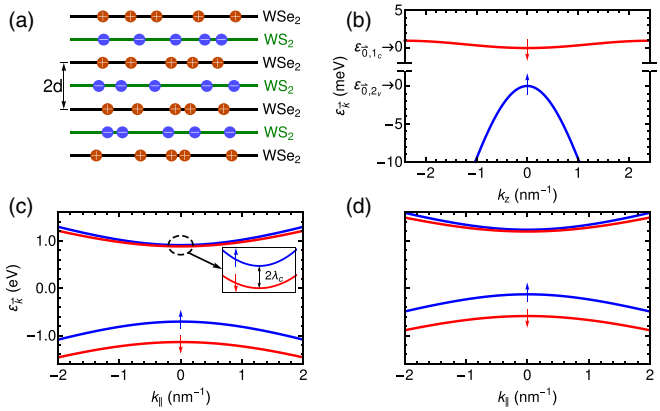

FIG. 1. (a) Schematic illustration of the WS_2/WSe_2 heterostructure superlattice of periodicity $2d$, of alternating monolayers of the two different TMDs, one type n doped (green lines) and the other p doped (black lines). (b) Lowest conduction band and highest valence band of the superlattice as a function of k_z, expressed relative to the center of the K valley. Blue and red bands are spin-up and spin-down bands, respectively. For the K' valley, the spins are reversed. (c) Bands predominantly associated with WS_2 as a function of $\boldsymbol{k}_\parallel$. Inset shows a close-up of the two spin-split WS_2 conduction bands, separated by $2\lambda_c = 27$ meV. (d) Bands predominantly associated with WSe_2 as a function of $\boldsymbol{k}_\parallel$.

than that for the corresponding 2D system, thus ensuring sufficiently long exciton lifetimes.

We use a hybrid continuum tight-binding approach to determine the band structure of the superlattice. The low-energy Hamiltonian for the superlattice is given in Eqs. (S1)–(S3) of the Supplemental Material [20]. The energy spectrum shown in Figs. 1(b)–1(d) and the corresponding eigenstates are obtained by numerically solving the eigenvalue equation of the 4×4 Hamiltonian, Eq. (S1). For a given spin and valley quantum number, the single-particle eigenstate for energy band β is $|\psi_{\vec{k},\beta}\rangle$. For the WS_2 monolayer conduction band, we need consider only the lowest conduction band, with spin down (up) for the K (K') valley [see Fig. 1(c)], since the band above will start to fill only for $T \gtrsim 300$ K. We label the corresponding superlattice band $\beta = 1_c$, referring to the dominant component in Eq. (S1). Similarly, for the valence band of the WSe_2 monolayer, the very large spin splitting means that we need consider only the highest valence band, with spin up (down) for the K (K') valley. We label the corresponding superlattice band $\beta = 2_v$. Because of the spin polarization in the valleys, the number of flavors for the electrons and holes comes only from the valley degeneracy, $g_v = 2$. Figure 1(b) shows the lowest conduction band and highest valence band of the WS_2/WSe_2 heterostructure superlattice as a function of the perpendicular wave vector component k_z, expressed relative to the center of the K valley. Blue and red bands are spin-up and spin-down bands, respectively. For the K' valley, the spins are reversed. Figures 1(c) and 1(d) show the bands associated predominantly with WS_2 and WSe_2, respectively, as a function of the in-plane wave vector component $\boldsymbol{k}_\parallel$, again relative to the K valley.

We will evaluate the bare Coulomb interaction matrix elements $\langle\psi_{\vec{k}',\alpha'}\psi_{\vec{k}',\beta'}|V|\psi_{\vec{k},\alpha}\psi_{\vec{k},\beta}\rangle$ for e-h scattering between the $|\psi_{\vec{k},\beta}\rangle$ eigenstates of the superlattice, with $V(r) = -e^2/(4\pi\varepsilon_r\varepsilon_0 r)$. The dielectric constant ε_r accounts for static screening effects of both ions and the filled valence bands. For bulk WS_2 $\varepsilon_r = \sqrt{\varepsilon_z\varepsilon_\parallel} = 9.9$, and for WSe_2 $\varepsilon_r = 11.2$ [21]. In the limit of no hybridization between the different TMD types, the system would effectively consist of two decoupled bulk TMDs with an interlayer distance twice that of their normal bulk forms. It is shown in Ref. [22] that the dielectric constant of MoS_2 is approximately halved when the interlayer distance is doubled. For the WS_2/WSe_2 superlattice, we therefore take as the value of the dielectric constant for the heterostructure superlattice $\varepsilon_r = 5.5$, half of the average of the two bulk TMDs. While the Keldysh potential [23] applies for monolayer TMDs, here the nature of the interactions in $\langle\psi_{\vec{k}',\alpha'}\psi_{\vec{k}',\beta'}|V|\psi_{\vec{k},\alpha}\psi_{\vec{k},\beta}\rangle$ is 3D and the average interparticle distances for the densities we are considering are much larger than the small distance between layers.

The interaction between electrons and holes from the same type TMD monolayers is given by [24,25]

$$V^{(0)}(\boldsymbol{q}_\parallel, q_z) = \frac{-e^2}{4\pi\varepsilon_r\varepsilon_0 NA}\frac{2\pi}{q_\parallel}\left[\frac{\sinh(2q_\parallel d)}{\cosh(2q_\parallel d) - \cos(2q_z d)}\right] \tag{1}$$

(for details see discussion in the Supplemental Material [20]). Equation (1) passes between the correct 2D and 3D limits (see Fig. S1). In the limit $d \to \infty$, the rightmost term is equal to unity, and we recover the 2D interaction potential for N layers of surface area A. In the limit $d \to 0$, a Taylor expansion of the trigonometric functions transforms the rightmost term to $2q_\parallel/[2d(q_\parallel^2 + q_z^2)]$, thus recovering the 3D interaction potential for volume $(AN2d)$.

For electrons and holes from different type TMD monolayers, we find that the interaction is

$$V^{(d)}(\boldsymbol{q}_\parallel, q_z) = \frac{-e^2}{4\pi\varepsilon_r\varepsilon_0 NA}\frac{2\pi}{q_\parallel}\left[\frac{2\sinh(q_\parallel d)\cos(q_z d)}{\cosh(2q_\parallel d) - \cos(2q_z d)}\right]. \tag{2}$$

In the limit $d \to 0$, Eq. (2) reduces to the standard 3D interaction potential, while the limit $d \to \infty$ introduces the familiar factor $2e^{-q_\parallel d}$.

When evaluating $\langle\psi_{\vec{k}',\alpha'}\psi_{\vec{k}',\beta'}|V|\psi_{\vec{k},\alpha}\psi_{\vec{k},\beta}\rangle$, it suffices to consider the dominant intraband interactions: $\alpha = \alpha' = 1_c$ and $\beta = \beta' = 2_v$ because of the large energy band gaps. For the superfluid calculations, e-h pairs with zero center-of-mass momentum are required for which the interaction is

$$\begin{aligned}&\left\langle\psi_{-\vec{k}',\alpha=1_c}\psi_{\vec{k}',\beta=2_v}\middle|V\middle|\psi_{-\vec{k},\alpha=1_c}\psi_{\vec{k},\beta=2_v}\right\rangle \\ &\quad= F^{(H)}_{\vec{k},\alpha;\vec{k}',\beta}V^{(0)}(\boldsymbol{q}_\parallel, q_z) + F^{(0)}_{\vec{k},\alpha;\vec{k}',\beta}V^{(d)}(\boldsymbol{q}_\parallel, q_z),\end{aligned} \tag{3}$$

with $\vec{q} = \vec{k} - \vec{k}'$. We represent 2D vectors in the x-y space of the monolayer planes as $\boldsymbol{k}_\parallel$, and vectors in 3D space as $\vec{k} \equiv (\mathbf{k}_\parallel, k_z)$. The form factors $F^{(H)}_{\vec{k},\alpha;\vec{k}',\beta}$ and $F^{(0)}_{\vec{k},\alpha;\vec{k}',\beta}$ are given in Eqs. (S7) of the Supplemental Material [20].

Equation (3) expresses the property that, due to the hybridization between the bands of the different type monolayers, there is a small intralayer contribution to the e-h potential. This is because, while the electrons and holes in the hybridized bands are mostly in opposite layers, there is a small

probability they will be in the same layer. At large momentum exchange $\boldsymbol{q}_\parallel$, the potential is dominated by 2D interactions between same type TMDs, $V^{(0)}(\boldsymbol{q}_\parallel, q_z)$, while at small $\boldsymbol{q}_\parallel$, the total interaction potential in Eq. (3) is dominated by 3D interactions between different type TMDs, $V^{(d)}(\boldsymbol{q}_\parallel, q_z)$ (see Fig. S1 in the Supplemental Material [20]). It is interesting to note that since pairing by the screened Coulomb attraction is primarily generated by two-particle scattering processes with small momentum exchange, pair formation is 3D in character.

Our interacting Hamiltonian for electrons and holes in the superlattice is

$$\mathcal{H} = \sum_{\vec{k}} (\varepsilon_{\vec{k},1_c} - \mu_e) c^\dagger_{\vec{k},1_c} c_{\vec{k},1_c} + (-\varepsilon_{\vec{k},2_v} - \mu_h) d^\dagger_{\vec{k},2_v} d_{\vec{k},2_v} + \sum_{\vec{k}\vec{k}'} \langle \psi_{-\vec{k}',1_c} \psi_{\vec{k}',2_v} | V | \psi_{-\vec{k},1_c} \psi_{\vec{k},2_v} \rangle c^\dagger_{-\vec{k}',1_c} d^\dagger_{\vec{k}',2_v} d_{\vec{k},2_v} c_{-\vec{k},1_c}. \tag{4}$$

We make the standard transformation for the holes in the valence band to positively charged particles with positive energies, so the chemical potentials μ_e and μ_h in the monolayers are both positive. $c^\dagger_{\vec{k},1_c}$ and $c_{\vec{k},1_c}$ ($d^\dagger_{\vec{k},2_v}$ and $d_{\vec{k},2_v}$) are the creation and destruction operators for the electrons (holes).

We use a self-consistent mean-field approach to determine the superfluid gap $\Delta(\vec{k})$ at zero temperature. To calibrate this approach, it has been tested against a full diffusion quantum Monte Carlo calculation for a 2D double-layer system [26]. The results for $\Delta(\vec{k})$ were found to be in excellent agreement.

In our 3D system, the zero-temperature $\Delta(\vec{k})$ is the self-consistent solution of

$$\Delta(\vec{k}) = -\sum_{\vec{k}'} V^{RPA}(\vec{k}, \vec{k}') \frac{\Delta(\vec{k}')}{2E_{\vec{k}'}}, \tag{5}$$

where $E_{\vec{k}} = \sqrt{\xi^2_{\vec{k}} + \Delta^2_{\vec{k}}}$, with $\xi_{\vec{k}} = \frac{1}{2}(\varepsilon_{\vec{k},1_c} - \varepsilon_{\vec{k},2_v}) - \mu$. We evaluate Eq. (5) at a fixed value of the average chemical potential $\mu = \frac{1}{2}(\mu_e + \mu_h)$. The terms in the summation over $\boldsymbol{k}'_\parallel$ are non-negligible only at low energies, but the summation over k'_z has significant contributions across the full Brillouin zone, i.e., between $\pm\pi/2d$. $V^{RPA}(\vec{k}, \vec{k}')$ is the self-consistent RPA screened e-h interaction in the superlattice in the presence of the superfluid. The screening is due to the polarization of the electron and hole densities and the superfluid condensate [5]. The expression for $V^{RPA}(\vec{k}, \vec{k}')$ is given by Eq. (S8) in the Supplemental Material [20].

For given values of the chemical potentials μ_e and μ_h, the 3D electron and hole densities are given by

$$n = \frac{g_v}{AN2d} \sum_{\vec{k}} (v_{\vec{k}})^2. \tag{6}$$

Note even though we set electron and hole densities n equal, $\mu_e \neq \mu_h$ because of the unequal effective masses.

Figure 2(a) shows the zero-temperature $\Delta^{\max}$, the maximum of the momentum-dependent superfluid gap $\Delta(\vec{k})$ [Eq. (5)], as a function of the 3D electron and hole densities n. For reference the top axis shows an effective 2D carrier density, defined as $n_{2D} = 2dn$. At large densities, Coulomb screening suppresses the superfluidity. Below an onset density n_0, large gap superfluidity self-consistently weakens the screening sufficiently for superfluidity to appear. As the density is further decreased, $\Delta^{\max}$ increases to a maximum value of 48 meV (560 K), and then decreases. Note that even for very small values of n, $\Delta^{\max}$ remains in excess of 10 meV (120 K). These large values of $\Delta^{\max}$ reflect the strong e-h Coulomb pairing interaction. Figure 2(b) shows the condensate fraction $\mathcal{C}$ that determines the density range for the BCS, BCS-BEC crossover, and BEC regimes [see Eq. (S11) of the Supplemental Material [20]].

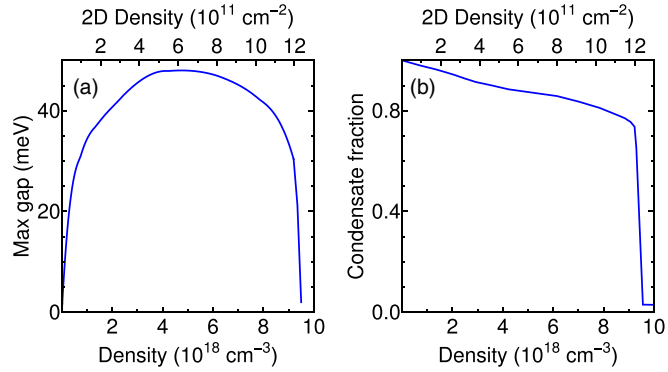

FIG. 2. (a) Maximum superfluid gap $\Delta^{\max}$ as a function of equal electron and hole densities n. Top axis shows effective 2D density n_{2D}. (b) Condensate fraction $\mathcal{C}$.

At high densities at weak coupling, the superfluid transition temperature T_c can be determined from the mean-field BCS equations, Eqs. (5) and (6), generalized to finite temperatures.

As the density is lowered, we enter the BCS-BEC crossover regime. With the increased pairing strength, the chemical potential μ must drop below the Fermi energy E_F to keep the density fixed. This drop incorporates a large part of the effect of the fluctuations that build up as the crossover regime is penetrated. Although within the crossover regime the T_c determined from the generalized Eqs. (5) and (6) using the self-consistent μ starts to overestimate the actual transition temperature, this overestimate is expected to be $\lesssim$20% across the full crossover regime [27,28]. For example, for ultracold fermions, the simplest non-self-consistent t-matrix approach overestimates the T_c obtained by quantum Monte Carlo (QMC) simulations by only ~20% at unitarity in the crossover regime (Fig. 3 of Ref. [28]). In this t-matrix approach, the sole ingredient entering the T_c calculation is the renormalization of the chemical potential.

In the self-consistent screening, we retain the superfluid gap at zero T, since the pseudogap arising from the pair fluctuations should remain of the order of $\Delta(T=0)$ in the intermediate coupling regime [29], and so to a large extent the low-lying excited states will continue to be excluded from the screening excitations, suppressing the detrimental Coulomb screening. In this way we take into account a major part of the fluctuation effects that renormalize T_c to lower values, by incorporating a large part of the fluctuations through the reduction of the chemical potential and through the development of the pseudogap.

This effective mean-field approach to determine the superfluid T_c is robust against fluctuation-driven suppression of T_c

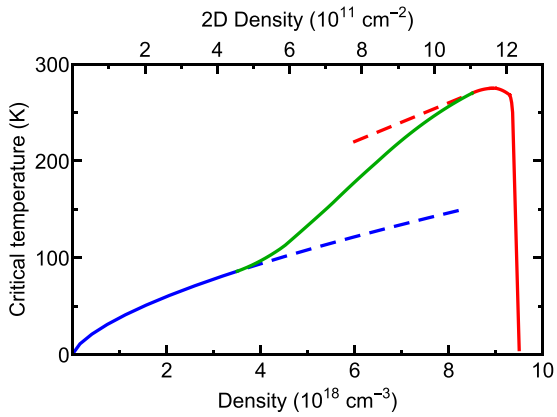

FIG. 3. Superfluid transition temperature T_c as a function of n, the equal electron and hole density in the superlattice. Red line: T_c determined in the BCS and BCS-BEC crossover regimes using Eqs. (5) and (6) generalized to finite temperatures. Blue line: T_c determined in the deep BEC regime using Eq. (S12) of the Supplemental Material [20]. Green line: interpolation.

arising from the strong anisotropy of the superlattice [30]. Reference [30] evaluates T_c across the BCS-BEC crossover regime for an anisotropic layered superfluid Fermi gas in an optical lattice, and includes Gaussian fluctuations beyond mean field. These fluctuations are expected to incorporate most of the suppression of T_c due to low-dimensional fluctuations in the superfluid when the dimensionality is lowered from 3D to 2D [31]. Figure 2 in Ref. [30] shows T_c in the BCS-BEC crossover regime for different values of the single-particle hopping anisotropy. It can be seen that near the maximum T_c, the regime of interest to us, a factor 10 in the anisotropy reduces T_c by less than 15%. The hopping anisotropy in our superlattice is of the order of ten, so we can conclude that the fluctuations associated with anisotropy have little effect on the T_c calculated within our effective mean-field approach described above, for the density range from the onset density to the crossover regime where our T_c passes through its maximum. It is interesting to note that we find the anisotropy of the superfluid near the optimal density is much smaller than the anisotropic ratio of the superlattice, consistent with the findings in Ref. [30].

In the deep BEC regime at low densities ($\mathcal{C} > 0.9$), this method for determining T_c becomes unreliable, primarily because the pseudogap is replaced by a real gap of the order of the pair binding energy. In the deep BEC, we can approximate the e-h pairs as pointlike bosons, so we can use the T_c for BEC of noninteracting bosons [Eq. (S12) of the Supplemental Material [20]]. The T_c thus obtained is known to underestimate the actual T_c for BEC as determined by QMC [32]. Finally, in the density range from the upper boundary of the BEC regime to the start of the deep BEC, we use a smooth interpolation of T_c between the high- and low-density results.

Figure 3 shows the resulting superfluid transition temperature in the superlattice. In the deep-BEC regime, T_c (blue curve) can approach 100 K, many orders of magnitude larger than the BEC transition temperatures found in ultracold-atom systems [33–35]. These BEC transition temperatures are so much larger because the effective electron and hole masses are tiny compared to atomic masses, and because our densities are several orders of magnitude larger than in ultracold-atom systems. Increasing the density causes T_c to rapidly rise, pushing it to a maximum in the BCS-BEC crossover regime (red curve) very close to room temperature, $T_c = 270$ K—conveniently accessible in a domestic refrigerator.

We do not expect that disorder or small density imbalance between layers would significantly affect our results for the following reasons. The effect of charged disorder on electron-hole superfluidity is similar to that of magnetic impurities in a superconductor, and for this reason closely related to the effect of density imbalance. Our superfluid results are confined to the BEC and BCS-BEC crossover regimes, and Ref. [36] showed for electrons and holes in GaAs double quantum wells, that in these regimes the superfluidity is not very sensitive to density imbalances even of 10%. Furthermore, the recent experimental observation of condensation at high T_c in electron-hole double TMD monolayers [8] is additional evidence that the effect of disorder will be weak, particularly since these observations are consistent with our theoretical predictions for the same TMD system which were calculated with no disorder [10]. The effect of disorder on T_c is not expected to be stronger in 3D than in 2D.

While for convenience our calculations use the realistic band structure of an infinite superlattice, our conclusions remain valid for corresponding finite superlattices consisting of more than a few monolayers [37]. To detect the superfluidity, a neutral supercurrent parallel to the superlattice layers that is uniform in the perpendicular direction, could be set up in a counterflow configuration by electrically contacting together the n-doped layers, and similarly with the p-doped layers. Alternatively, a capacitance spectroscopy measurement [38] could detect the drop in density of states for the superfluid state relative to the normal state. The onset of superfluidity will be characterized by a jump in the inverse of the total capacitance across the sample [39], and then as the density is decreased, this will monotonically increase.

Our results open the way to generating 3D e-h superfluidity at room temperature in this and related superlattices.

This work was supported by the Research Foundation of Flanders (FWO-Vl) through an aspirant research grant for M.V.d.D., by the FLAG-ERA project TRANS-2D-TMD, and by the Australian Government through the Australian Research Council Centre of Excellence in Future Low-Energy Electronics (Project No. CE170100039). We thank Milorad V. Milošević, Pierbiagio Pieri, and Jacques Tempere for helpful discussions.

[1] L. V. Keldysh and Y. V. Kopaev, Possible instability of semimetallic state toward Coulomb interaction, Sov. Phys. Solid State, USSR **6**, 2219 (1965).

[2] Y. E. Lozovik and V. I. Yudson, Feasibility of superfluidity of paired spatially separated electrons and holes, JETP Lett. (USSR) **22**, 274 (1975) [Pis'ma Zh. Eksp. Teor. Fiz. **22**, 556 (1975)].

[3] P. Rivera, H. Yu, K. L. Seyler, N. P. Wilson, W. Yao, and X. Xu, Interlayer valley excitons in heterobilayers of transition metal dichalcogenides, Nat. Nanotechnol. **13**, 1004 (2018).

[4] H. Min, R. Bistritzer, J.-J. Su, and A. H. MacDonald, Room-temperature superfluidity in graphene bilayers, Phys. Rev. B **78**, 121401(R) (2008).

[5] A. Perali, D. Neilson, and A. R. Hamilton, High-Temperature Superfluidity in Double-Bilayer Graphene, Phys. Rev. Lett. **110**, 146803 (2013).

[6] G. W. Burg, N. Prasad, K. Kim, T. Taniguchi, K. Watanabe, A. H. MacDonald, L. F. Register, and E. Tutuc, Strongly Enhanced Tunneling at Total Charge Neutrality in Double-Bilayer Graphene-WSe_2 Heterostructures, Phys. Rev. Lett. **120**, 177702 (2018).

[7] D. K. Efimkin, G. W. Burg, E. Tutuc, and A. H. MacDonald, Tunneling and fluctuating electron-hole Cooper pairs in double bilayer graphene, Phys. Rev. B **101**, 035413 (2020).

[8] Z. Wang, D. A. Rhodes, K. Watanabe, T. Taniguchi, J. C. Hone, J. Shan, and K. F. Mak, Evidence of high-temperature exciton condensation in two-dimensional atomic double layers, Nature (London) **574**, 76 (2019).

[9] A. Chaves and D. Neilson, Two-dimensional semiconductors host high-temperature exotic state, Nature (London) **574**, 39 (2019).

[10] S. Conti, M. Van der Donck, A. Perali, F. M. Peeters, and D. Neilson, Doping-dependent switch from one- to two-component superfluidity in coupled electron-hole van der Waals heterostructures, Phys. Rev. B **101**, 220504(R) (2020).

[11] N. D. Mermin and H. Wagner, Absence of Ferromagnetism or Antiferromagnetism in One- or Two-Dimensional Isotropic Heisenberg Models, Phys. Rev. Lett. **17**, 1133 (1966).

[12] P. C. Hohenberg, Existence of long-range order in one and two dimensions, Phys. Rev. **158**, 383 (1967).

[13] J. M. Kosterlitz and D. J. Thouless, Ordering, metastability and phase transitions in two-dimensional systems, J. Phys. C: Solid State **6**, 1181 (1973).

[14] Y. E. Lozovik, S. L. Ogarkov, and A. A. Sokolik, Condensation of electron-hole pairs in a two-layer graphene system: Correlation effects, Phys. Rev. B **86**, 045429 (2012).

[15] M. D. Croitoru and A. I. Buzdin, Extended Lawrence-Doniach model: The temperature evolution of the in-plane magnetic field anisotropy, Phys. Rev. B **86**, 224508 (2012).

[16] L. B. Ioffe and A. J. Millis, Superconductivity and the c axis spectral weight of high-T_c superconductors, Science **285**, 1241 (1999).

[17] D. G. Clarke and S. P. Strong, Confined coherence in strongly correlated anisotropic metals, Adv. Phys. **46**, 545 (1997).

[18] H. Terrones, F. López-Urías, and M. Terrones, Novel hetero-layered materials with tunable direct band gaps by sandwiching different metal disulfides and diselenides, Sci. Rep. **3**, 1549 (2013).

[19] P. Rivera, J. R. Schaibley, A. M. Jones, J. S. Ross, S. Wu, G. Aivazian, P. Klement, K. Seyler, G. Clark, N. J. Ghimire, J. Yan, D. G. Mandrus, W. Yao, and X. Xu, Observation of long-lived interlayer excitons in monolayer $MoSe_2$-WSe_2 heterostructures, Nat. Commun. **6**, 6242 (2015).

[20] See Supplemental Material at http://link.aps.org/supplemental/10.1103/PhysRevB.102.060503 for further technical details on the superlattice Hamiltonian and e-h interaction potential, which includes Refs. [5,18].

[21] A. Laturia, M. L. Van de Put, and W. G. Vandenberghe, Dielectric properties of hexagonal boron nitride and transition metal dichalcogenides: From monolayer to bulk, npj 2D Mater. Appl. **2**, 6 (2018).

[22] T. C. Berkelbach, M. S. Hybertsen, and D. R. Reichman, Theory of neutral and charged excitons in monolayer transition metal dichalcogenides, Phys. Rev. B **88**, 045318 (2013).

[23] L. V. Keldysh, Coulomb interaction in thin semiconductor and semimetal films, JETP Lett. **29**, 658 (1979) [Pis'ma Zh. Eksp. Teor. Fiz. **29**, 716 (1979)].

[24] A. L. Fetter, Electrodynamics of a layered electron gas. II. Periodic array, Ann. Phys. **88**, 1 (1974).

[25] V. N. Kotov, B. Uchoa, V. M. Pereira, F. Guinea, and A. H. Castro Neto, Electron-electron interactions in graphene: Current status and perspectives, Rev. Mod. Phys. **84**, 1067 (2012).

[26] P. López Ríos, A. Perali, R. J. Needs, and D. Neilson, Evidence from Quantum Monte Carlo Simulations of Large-Gap Superfluidity and BCS-BEC Crossover in Double Electron-Hole Layers, Phys. Rev. Lett. **120**, 177701 (2018).

[27] R. Haussmann, Properties of a Fermi liquid at the superfluid transition in the crossover region between BCS superconductivity and Bose-Einstein condensation, Phys. Rev. B **49**, 12975 (1994).

[28] M. Pini, P. Pieri, and G. Calvanese Strinati, Fermi gas throughout the BCS-BEC crossover: Comparative study of t-matrix approaches with various degrees of self-consistency, Phys. Rev. B **99**, 094502 (2019).

[29] A. Perali, P. Pieri, G. C. Strinati, and C. Castellani, Pseudogap and spectral function from superconducting fluctuations to the bosonic limit, Phys. Rev. B **66**, 024510 (2002).

[30] M. Iazzi, S. Fantoni, and A. Trombettoni, Anisotropic Ginzburg-Landau and Lawrence-Doniach models for layered ultracold Fermi gases, Europhys. Lett. **100**, 36007 (2012).

[31] A. Larkin and A. Varlamov, *Theory of fluctuations in superconductors*, International series of monographs on physics (Clarendon, Oxford, 2005).

[32] E. Burovski, E. Kozik, N. Prokof'ev, B. Svistunov, and M. Troyer, Critical Temperature Curve in BEC-BCS Crossover, Phys. Rev. Lett. **101**, 090402 (2008).

[33] M. H. Anderson, J. R. Ensher, M. R. Matthews, C. E. Wieman, and E. A. Cornell, Observation of Bose-Einstein condensation in a dilute atomic vapor, Science **269**, 198 (1995).

[34] C. C. Bradley, C. A. Sackett, J. J. Tollett, and R. G. Hulet, Evidence of Bose-Einstein Condensation in an Atomic Gas with Attractive Interactions, Phys. Rev. Lett. **75**, 1687 (1995).

[35] K. B. Davis, M. O. Mewes, M. R. Andrews, N. J. van Druten, D. S. Durfee, D. M. Kurn, and W. Ketterle, Bose-Einstein Condensation in a Gas of Sodium Atoms, Phys. Rev. Lett. **75**, 3969 (1995).

[36] P. Pieri, D. Neilson, and G. C. Strinati, Effects of density imbalance on the BCS-BEC crossover in semiconductor electron-hole bilayers, Phys. Rev. B **75**, 113301 (2007).

[37] B. Partoens and F. M. Peeters, From graphene to graphite: Electronic structure around the K point, Phys. Rev. B **74**, 075404 (2006).

[38] M. J. Yang, C. H. Yang, B. R. Bennett, and B. V. Shanabrook, Evidence of a Hybridization Gap in "Semimetallic" InAs/GaSb Systems, Phys. Rev. Lett. **78**, 4613 (1997).

[39] S. Saberi-Pouya, S. Conti, A. Perali, A. F. Croxall, A. R. Hamilton, F. M. Peeters, and D. Neilson, Experimental conditions for the observation of electron-hole superfluidity in GaAs heterostructures, Phys. Rev. B **101**, 140501(R) (2020).